DESIGN AND EXPERIMENTAL STUDY OF A HIGH GROUND CLEARANCE WEEDING ROBOT CHASSIS
/
高地隙跨垄除草机器人底盘设计与试验

Wentao XU, Lei HAN, Yanhua MA, Tao LIU, Wen LIU
Inner Mongolia Agricultural University, College of Mechanical and Electrical Engineering, Inner Mongolia, China;
[1]Tel: 0471-4309215; E-mail: hanlei@imau.edu.cn
Corresponding author: Lei Han; Tao Liu
DOI: https://doi.org/10.35633/inmateh-75-93

Keywords: *high ground clearance weeding robot; inter-row chassis design; stability analysis; field test*

ABSTRACT

This study addresses the inefficiency, high crop damage, and poor adaptability of traditional cornfield weeding machinery. A High-Clearance Inter-Row Weeding Robot Chassis was developed and tested through simulations and experiments. With a refined suspension and floating wheels, it achieves 800 mm ground clearance for dual-row weeding. Simulations show maximum chassis stresses of 124.7 MPa and 134.88 MPa under sharp turns and braking. Stability assessments indicate theoretical climb angles of 26.5° longitudinally and 35° transversely, with experimental test results of 22° and 32°, respectively. The robot operates at speeds exceeding 0.8 m/s, overcomes obstacles of up to 370 mm, and traverses trenches narrower than 350 mm or wider than 600 mm. Results confirm its stability, obstacle-crossing ability, and precision, offering a viable solution for intelligent weeding in complex fields.

摘要

本研究针对传统玉米田除草机械存在的低效率、高作物损伤率和适应性差等问题，研制并测试了一种高离地间隙的行间除草机器人底盘。通过设计浮动轮悬架结构，该底盘实现了 800 mm 的离地间隙，可用于双行除草。仿真结果表明，在急转弯和制动工况下，底盘的最大应力分别为 124.7 MPa 和 134.88 MPa。稳定性评估显示，理论纵向爬坡角为 26.5°，横向爬坡角为 35°，实际测试结果分别为 22° 和 32°。机器人运行速度大于 0.8 m/s，可跨越 370 mm 高的障碍物，并可通过宽度小于 350 mm 或大于 600 mm 的沟渠。结果表明，该机器人具备较高的稳定性、优异的越障能力和精确的作业性能，为复杂农田环境下的智能除草提供了一种可行方案。

INTRODUCTION

Weed infestation significantly impacts crop production by competing for resources such as water, nutrients, light, and space, especially during the seedling stage. Weeds hinder crop growth, reducing yields and potentially causing crop failure. While chemical weeding is effective, it poses risks to food security, and manual weeding is labor-intensive and inefficient. Intelligent weeding robots could provide a viable solution (*Upadhyay et al., 2024; Yang, L. et al., 2023; Zhang, Z. et al., 2024*).

Research on domestic weeding robots is mainly conducted by academic institutions. For example, Xin Li from Northeast Agricultural University designed a tracked weeding robot for paddy fields. Wei Li's team at China Agricultural University developed a tractor-drawn robot with crescent-shaped hoes and machine vision for efficient weeding. Liang'an Zhang from Anhui University of Technology created a four-legged laser weeding robot, offering better mobility and adaptability. Additionally, researchers at Nanjing Forestry University designed a robot for targeted pesticide application. However, most of these robots are limited to inter-row operation and have small payloads and short battery life (*Bručienė et al., 2022; Guo, 2022; Hussain et al., 2023; Mao, 2020; Zhang L. et al., 2020*).

To address labor intensity, plant damage, soil compaction, and the limitations of traditional methods, developing a high-clearance inter-row intelligent weeding robot is essential for improving precision in field operations.

Wentao Xu, M.E. Chn.; Lei Han, Prof. Ph.D. Chn.; Yanhua Ma, Prof. Chn.; Tao Liu, Prof Chn; Wen Liu, M.E. Chn.

MATERIALS AND METHODS

Suspension System Design

To enhance the robot's adaptability to complex operating environments and improve its off-road performance, the chassis suspension incorporates a front-and-rear cross-floating design. The two side wheels are mounted on a cross axle, and each wheel is equipped with an independent shock-absorbing damper, enabling vertical movement and rotational flexibility within a defined range around the cross axle. Furthermore, to prevent forward or backward tilting of the robot's body, the left and right cross arms are interconnected via linkages and a balance bar (*Băzăvan and Ionita, 2024; Yao et al., 2023; Zhao et al., 2024*). The installation configuration of the entire suspension system is presented in figure 1.

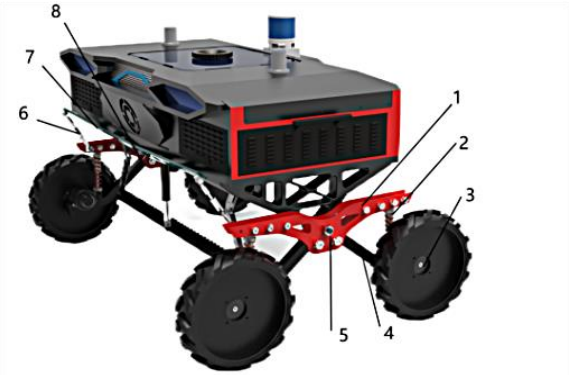

Fig. 1 – Installation position of the weeding robot suspension system

1. Side cross-arm; 2. Shock absorber; 3. Wheel; 4. Suspension lower arm; 5. Cross axle; 6. Connecting rod; 7. Balance bar; 8. Balance bar axle

Robot Chassis Stability Analysis

In SolidWorks, appropriate materials are assigned to each component of the robot, and their mass properties are analyzed to determine the robot's overall center of mass and center of gravity (*Tao, 2024*). Figure 2 illustrates the robot platform in a fully loaded state. The height of the center of gravity from the ground is approximately 730 mm. As shown in figure 3, the distance from the center of gravity to the front wheel axle is 370mm, while the distance to the rear wheel axle is 443mm.

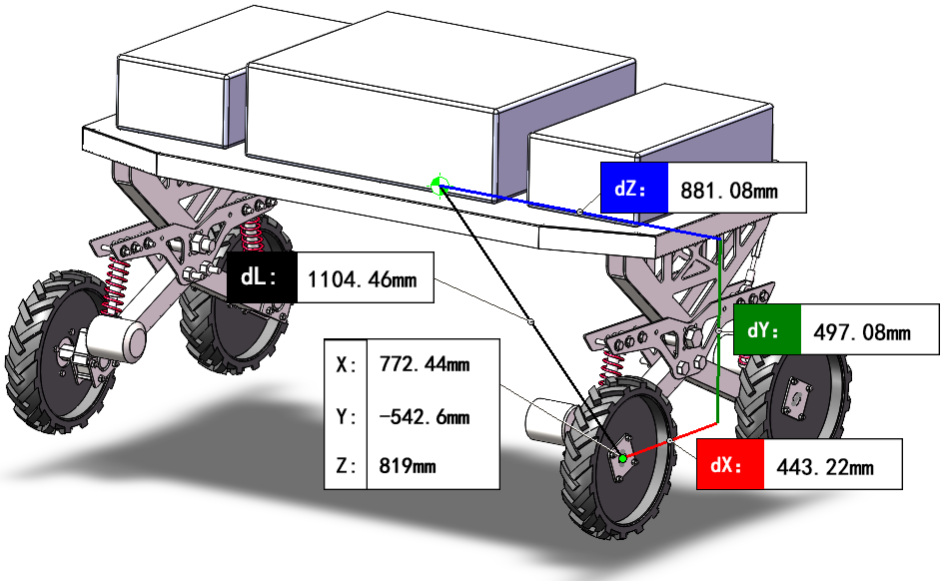

Fig. 2 – Relative position of the center of gravity and front axle under full-load conditions

Longitudinal stability analysis

When the robot operates on a field or roadway slope (moving along the slope), excessive slope angles may lead to longitudinal slip or overturning.

During actual operation, the robot's slow speed allows the effects of inertia, air resistance, and sliding resistance on its motion to be neglected (*Mou et al., 2023; Zhou et al., 2024*).

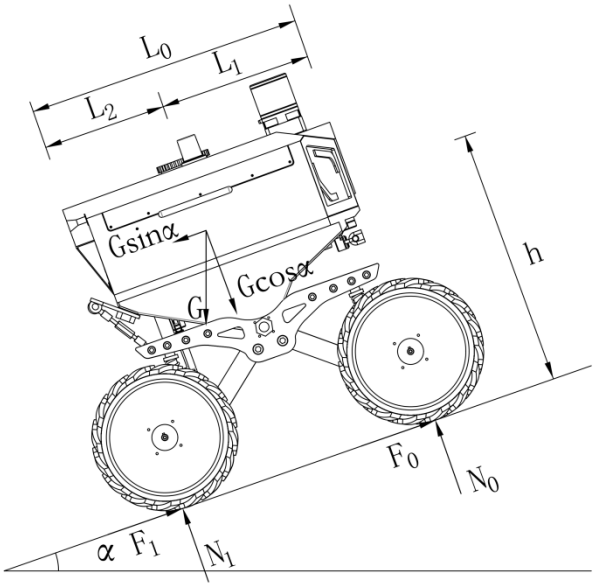

Fig. 3 – Schematic diagram of force distribution during longitudinal movement

As illustrated in figure 3, L_0 denotes the distance between the front and rear wheel axles of the high ground clearance, inter-row weeding robot; L_1 represents the distance from the robot's center of gravity to the front wheel axle center; L_2 is the distance from the center of gravity to the rear wheel axle center; G signifies the robot's weight; θ is the longitudinal slope angle; h is the height of the center of gravity; F_1 and F_2 are the tangential reaction forces at the contact points of the front and rear wheels, respectively; and N_0 and N_1 are the normal reaction forces at the contact points of the front and rear wheels, respectively.

(1) Conditions for Longitudinal Overturning

When the robot operates on a slope, the standard and tangential reaction forces acting on the front wheel are influenced by the terrain and slope angle. Longitudinal overturning occurs when these reaction forces reduce to zero (N_0=0, F_0=0), causing the robot to pivot around the rear wheel's contact point with the ground. The critical condition for longitudinal overturning is defined by the limit equilibrium equation at this point:

$$G\cos\alpha_1 \cdot L_2 - G\sin\alpha_1 \cdot h = 0 \tag{1}$$

Simplified, it becomes (2):

$$i_1 = \tan\alpha_1 = \frac{L_2}{h} \tag{2}$$

where:

G - Gravity acting on the robot; i_1 - longitudinal rollover stability; α_1 - slope angle, [°]; h - height of the center of gravity, [mm]; L_2 - distance from the robot's center of gravity to the rear axle along the direction of travel, [mm].

From the equation, both the height of the center of gravity and its distance from the wheel axles influence overturning stability. A greater distance between the center of gravity and the rear wheel axle increases the maximum climbing overturning angle, while a greater distance from the front wheel axle enhances the maximum descending overturning angle. When the longitudinal slope angle remains below the robot's overturning limit, the high ground clearance weeding robot maintains stability without overturning.

(2) Conditions for Longitudinal Sliding

During operation on a longitudinal slope, the robot may also experience wheel slip. The critical balance condition for longitudinal sliding is expressed as:

$$G\sin\alpha_2 - P_k\mu = 0 \tag{3}$$

where:

P_K - driving load on the robot's wheels, [N]; μ - road adhesion coefficient.

$$P_K = G\cos\alpha_2 \tag{4}$$

Substituting the values, it will result:

$$i_2 = \tan\alpha_2 = \mu \tag{5}$$

where:

i_2 - longitudinal slip stability; α_2 - critical angle for longitudinal slip, [°]; μ - adhesion coefficient.

According to the formula, longitudinal sliding stability depends on the coefficient of friction between the ground and the tires. When the slope angle is below the critical sliding angle, the robot operates normally. However, if the slope angle exceeds this critical value, the robot loses traction, leading to longitudinal sliding and reduced stability.

Transverse stability analysis

When the high ground clearance inter-row weeding robot operates transversely on a slope, a height difference may arise between its left and right sides, potentially resulting in transverse overturning or sliding. Neglecting the influences of air resistance, inertial resistance, and rolling resistance during the robot's motion, the force analysis of the robot moving transversely on a slope is illustrated in figure 4.

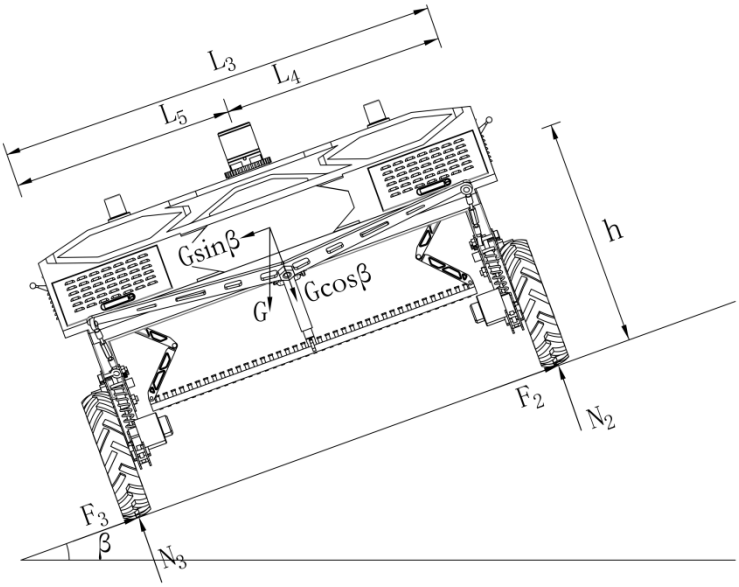

Fig. 4 - Schematic of transverse forces during travel

(1) Conditions for Transverse Overturning of the high ground clearance Inter-Row Weeding Robot

When the robot undergoes transverse overturning while traversing a slope, the standard and tangential reaction forces on the upper wheels reduce to zero. The robot will then rotate around the contact point between the lower wheel and the ground, leading to overturning. The critical balance equation for transverse overturning is as follows:

$$G\sin\beta_1 \cdot h - G\cos\beta_1 \cdot L_5 = 0 \tag{6}$$

Simplified, it becomes:

$$i_3 = \tan\beta_1 = \frac{L_5}{h} \tag{7}$$

where:

i_3 - denotes the transverse overturning stability; L_5 - represents the horizontal distance from the center of gravity to the lower wheel, [mm]; β_1 - indicates the slope angle, [°]; h - corresponds to the vertical distance from the center of gravity to the ground, [mm].

From the above equation, it is evident that both the height of the center of gravity and the horizontal distance from the center of gravity to the lower wheel significantly influence transverse overturning stability.

For a fixed track width, a lower center of gravity and a greater horizontal distance between the center of gravity and the lower wheel result in a larger critical angle for transverse overturning. Consequently, the risk of transverse overturning is reduced, thereby enhancing the robot's transverse stability.

(2) Conditions for Transverse Sliding of the high ground clearance Inter-Row Weeding Robot

In addition to the risk of overturning, transverse movement of the robot on slopes may also result in sliding. When the robot approaches the critical sliding condition, the limit equilibrium equation can be expressed as:

$$i_3 = \tan \beta_2 = \frac{L_5}{h} \tag{8}$$

Simplified, it becomes:

$$i_4 = \tan \beta_2 = \mu' \tag{9}$$

where:

i_4 - denotes transverse sliding stability; β_2 - represents the slope angle in degrees, [°]; μ' - transverse adhesion coefficient.

From this equation, it is evident that the robot can maintain normal transverse operation without slipping when the slope angle is smaller than the sliding angle.

Chassis Structural Strength Analysis

Analysis of Emergency Turning Conditions and Result Interpretation

During emergency turning maneuvers, transverse forces are exerted on the chassis frame components, generating transverse loads (*Dharma et al., 2024; Dudescu et al., 2023; Kiran, 2024; Deulgaonkar et al., 2022*). Given the robot's relatively low maximum speed, the centrifugal acceleration was set to 0.2g, based on its minimum turning radius and maximum operating speed. This results in transverse inertial forces acting on the chassis frame and its components. The load and constraints under steady-state driving conditions remain unchanged, with the inertial force applied in the direction of centrifugal force. The force magnitude is calculated as F=0.2g, where M represents the combined mass of the battery and water tank.

The analysis results for the emergency turning condition are shown in figure 5. The maximum stress of 124.7 MPa occurs at the contact point between the main beam of the platform's upper plate frame and the vertical side plate. The deformation contour map indicates a maximum deformation of 1.71 mm, which satisfies the strength requirements.

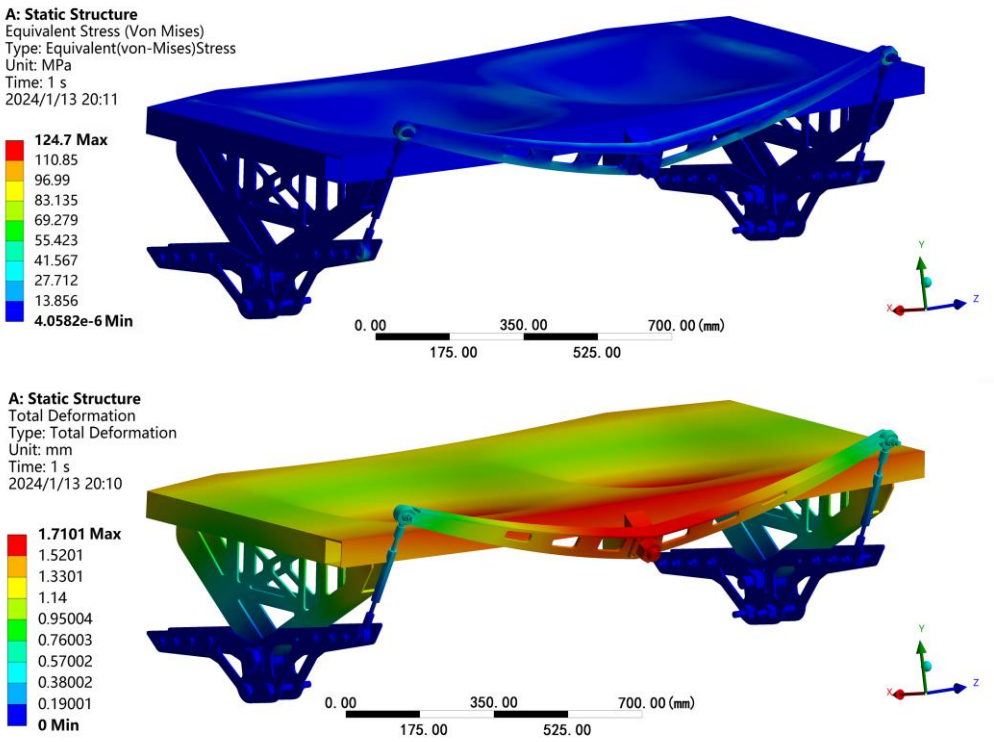

Fig. 5 - Analysis results of emergency turning conditions

Analysis of Emergency Braking Conditions and Result Interpretation

During field operations, the high ground clearance Inter-Row Weeding Robot may undergo emergency braking or reverse operation. In such scenarios, the chassis frame experiences significant inertial loads, acting in the direction opposite to the motion. The braking acceleration was estimated based on the robot's maximum speed, with the load and constraints under steady-state driving conditions remaining unchanged. The inertial force, applied to the upper components, acts opposite to the direction of motion. The braking acceleration was set to 0.4g, and the inertial force magnitude was calculated as F=0.4g, where M represents the combined mass of the battery and water tank.

The analysis results for the emergency braking condition are shown in figure 6. The maximum stress of 134.88 MPa occurs at the connection between the tie rod and the middle balance connecting rod. The deformation contour map shows a maximum deformation of 4.52 mm on the upper plate of the chassis, primarily attributed to the large 125 l pesticide tank mounted on the upper side.

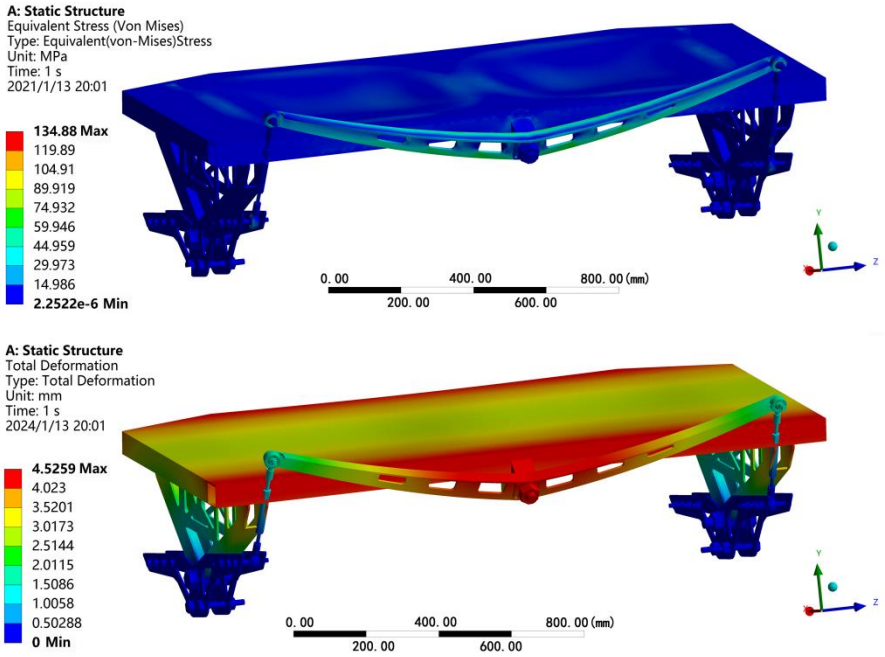

Fig. 6 - Analysis results of braking conditions

RESULTS

Weeding Robot Speed Test

Based on the theoretical design specifications, the high ground clearance Inter-row Weeding Robot achieves a speed exceeding 0.8 m/s on flat terrain. To validate whether the robot meets the theoretical speed requirements, a 50-meter test section on a flat farm road was selected. The robot's forward and reverse speeds were measured at both 50% and 100% throttle settings. The detailed testing procedure is illustrated in figure 7 (*Cen, 2023; Jiang et al., 2023; Yang Z., 2023*).

Fig. 7 - Test diagram of the weeding robot's deviation rate

Table 1

Test Results of the Weeding Robot's Speed on Field Terrain

Test number	Forward				Reverse			
	50% Throttle		100% Throttle		50% Throttle		100% Throttle	
	Time of the experiment (s)	Speed (m/s)	Time of the experiment (s)	Speed (m/s)	Time of the experiment (s)	Speed (m/s)	Time of the experiment (s)	Speed (m/s)
1	84.3	0.593	56.8	0.880	85.2	0.587	55.4	0.923
2	83.5	0.600	57.4	0.871	84.8	0.590	56.8	0.880
3	83.8	0.597	55.1	0.907	86.9	0.575	56.4	0.887
Average	**83.87**	**0.596**	**56.4**	**0.887**	**85.63**	**0.584**	**56.2**	**0.890**

As presented in Table 1, the average forward speed at 50% throttle is 0.596 m/s, while the reverse speed is 0.584 m/s. At full throttle (100%), the average forward and reverse speeds increase to 0.887 m/s and 0.890 m/s, respectively. These results indicate that the welding robot's operational speed on field roads complies with the design specifications.

Weeding Robot Obstacle-Crossing Performance Test

The high ground clearance Inter-Row Weeding Robot may encounter obstacles such as potholes or uneven terrain during field operations. To address these challenges, the robot is equipped with a specialized suspension system featuring independent suspension on all four wheels and cross arms on both sides. The four-wheel drive configuration ensures continuous ground contact for all wheels during obstacle traversal. To validate the effectiveness of this mechanism, the robot's obstacle-crossing performance must be experimentally evaluated to determine its maximum obstacle-crossing capacity.

(1) Single Wheel Vertical Obstacle Test

This test simulates scenarios where the robot encounters sudden obstacles, such as rocks or raised surfaces, as well as more considerable obstacles during regular operation. A brick is utilized to replicate these obstacles, with each brick having a thickness of approximately 50 mm. By stacking multiple bricks, obstacles of varying heights are simulated. The robot is gradually driven toward the vertical obstacle and attempts to traverse it. The height of the obstacle is incrementally increased until the chassis is no longer capable of crossing. The results are documented in Table 2.

Table 2

Single Wheel Vertical Obstacle Test

Test number	Obstacle height [mm]	Crossing Result
1	53	Passed
2	106	Passed
3	159	Passed
4	212	Passed
5	265	Passed
6	318	Passed
7	371	Passed
8	424	Failed

Fig. 8 - Aspects from the experiment of crossing vertical obstacles with a single wheel of the weeding robot

(2) Single Wheel Trench Crossing Test

This experiment simulates scenarios in which the weeding robot encounters depressions or trenches in the field. The study evaluates the robot's trench-crossing capability by testing its performance on artificially dug trenches of varying widths. The trench width is incrementally increased until the robot fails to cross, and the corresponding data are recorded in Table 3.

Table 3

Single-Wheel Trench Crossing Experiment

Test number	Trench width [mm]	Through the effect
1	200	Passed
2	250	Passed
3	300	Passed
4	350	Passed
5	400	Failed
6	450	Failed
7	500	Failed
8	550	Failed
9	600	Passed
10	650	Passed

Fig. 9 - Aspects from the experiment of the Weeding Robot's single-wheel trench crossing

The robot is capable of surmounting vertical obstacles with a maximum height of 371 mm. However, its trench-crossing performance varies depending on trench width: it can effectively traverse trenches narrower than 350 mm or wider than 600 mm. When the trench width is between 400 mm and 550 mm, the ditch width is close to the wheel diameter. When the wheels come into contact with the ditch walls, they are prone to slipping, resulting in temporary entrapment.

Experimental results demonstrate that the suspension system significantly improves the robot's obstacle-crossing capabilities by ensuring continuous ground contact for all four wheels during the traversal process.

Stability Test of the Chassis Platform of the Weeding Robot

During field operations, the high-ground clearance weeding robot encounters sloped terrain, an evaluation of its stability to determine the maximum operational angles and suitable working environments being necessary. To replicate real-world conditions, the robot was positioned on a slope board at various incline angles. The water tank was filled, and additional weights were applied to the battery compartment to simulate the actual load distribution during operation. The robot's tipping and slipping thresholds were recorded under these conditions, as illustrated in figure 10.

Fig. 10 - Stability test of the Weeding Robot

For the high-clearance Inter-Row Weeding Robot, the position of the center of gravity is shown in figure 2. After calculation, i_1=0.602, and the friction coefficient μ=0.5. Thus, it is determined that $i_1 \geq i_2$. This indicates that when the robot travels on a slope, sliding occurs before overturning. The critical climbing angle is 26.5°. By calculation, i_3=1.14, and the typical dynamic friction coefficient is 0.71. Thus, it is determined that $i_3 \geq i_4$. This indicates that sliding occurs first when the robot moves laterally on a slope, and the maximum operating angle is 35°.

The stability test results, summarized in Table 4, reveal that the maximum slope climb angle for longitudinal movement is 22°, while the robot can achieve up to 32° for transverse (horizontal) movement. A discrepancy exists between the measured values and theoretical calculations, primarily attributed to differences between the slope board surface and actual field conditions. Furthermore, theoretical analyses assume ideal conditions, such as rigid robot components and constant friction coefficients, which are seldom encountered in practical scenarios. As indicated in Table 4, the robot demonstrates a higher maximum climb angle during transverse (horizontal) movement compared to vertical (uphill) movement, highlighting its enhanced stability and reduced likelihood of slipping during field operations.

Table 4

Stability Test Results

Test Item	Theoretical Value (°)	Actual Value (°)	Instability Type
Longitudinal Climb Angle	26.5	22	Slipping
Transverse Climb Angle	35	32	Slipping

CONCLUSIONS

1. A high-clearance, floating-wheel weeding robot was developed for weed control in maize seedling stages under complex field conditions. The robot features a floating suspension, electric drive, and differential steering, with a wheelbase of 1,800 mm. It can cover two rows of crops in a single pass. Static analysis using Ansys revealed maximum stress values of 124.7 MPa during braking and 134.88 MPa during turning, with corresponding deformations of 1.71 mm and 4.52 mm. These results confirm that the chassis meets the required specifications.

2. A stability analysis was conducted on the high-ground-clearance cross-row floating wheel weeding robot chassis system. The theoretical maximum climb angles for longitudinal and transverse movement on slopes were determined to be 26.5° and 35°, respectively.

3. Field experiments were conducted to evaluate the chassis of the weeding robot. The results demonstrated an average field travel speed exceeding 0.8 m/s. The robot could overcome vertical obstacles up to 371 mm in height on a single wheel. Additionally, it successfully traversed ditches with widths below 350 mm and above 600 mm. Stability tests revealed maximum climb angles of 22° for longitudinal movement and 32° for transverse movement.

REFERENCES

[1] Băzăvan, A., & Ioniță, E.R. (2024). Versatile multi-axis chassis a solution for rescue operations and mobility. *Journal of Information Systems & Operations Management*, Vol. 18(1), Romania.

[2] Bručienė, I., Buragienė, S., & Šarauskis, E. (2022). Weeding effectiveness and changes in soil physical properties using inter-row hoeing and a robot. *Agronomy*, Vol. 12, pp. 1514, Switzerland.

[3] Cen, H. (2023). Design and testing of a small agricultural robot for high-ridge and furrow environments (高垄畦沟小型农业作业机器人设计与试验). *Journal of Anhui Agricultural Sciences*, 51(23), 198–202, 237.

[4] Dharma, MD, Bhavya, G., Nithin, R., Jagadeesh, Y., & Shashivardhan, G. (2024). Design and analysis of automotive chassis frame using finite element method. *International Journal of Mechanical Engineering Research and Technology*, Vol. 16(2), pp. 512-518, India.

[5] Deulgaonkar, V. R., Deshpande, S., Bengle, A., & Dhanawade, P. (2022). Finite Element Analysis of Foldable Electric Vehicle. *International Journal of Vehicle Structures & Systems (IJVSS)*, 14(6).

[6] Dudescu, M.C., Paul, B., & Neamțu, C. (2023). Structural analysis of an electric car chassis by numerical and experimental methods. *Acta Technica Napocensis-Series: Applied Mathematics, Mechanics, and Engineering*, Vol. 65(4S), Romania.

[7] Guo, J.J. (2022). *Design and key technology research of a bow-shaped agricultural robot (弓腰式农业机器人设计及关键技术研究)*. Master's Thesis, Henan University of Science and Technology, Luoyang, China.

[8] Hussain, A., Fatima, H. S., Zia, S. M., Hasan, S., Khurram, M., Stricker, D., & Afzal, M. Z. (2023). Development of cost-effective and easily replicable robust weeding machine—premiering precision agriculture in Pakistan. *Machines*, Vol. 11, pp. 287, Switzerland.

[9] Jiang, W., Quan, L., Wei, G., Chang, C., & Geng, T. (2023). A conceptual evaluation of a weed control method with post-damage application of herbicides: A composite intelligent intra-row weeding robot. *Soil and Tillage Research*, Vol. 234, pp. 105837, Netherlands.

[10] Kiran, B. N. (2024). Structural optimization of four-wheeler chassis. *International Journal of Mechanical Engineering and Technology (IJMET)*, Vol. 15(4), pp. 30-53, India.

[11] Mao, T. (2020). *Design and experimental study of a walking platform for paddy field operation robots (水田作业机器人行走平台设计与试验研究)*. Master's Thesis, South China Agricultural University, Guangzhou, China.

[12] Mou, X., Luo, Q., Ma, G., Wan, F., He, C., Yue, Y., ... & Huang, X. (2023). Simulation Analysis and Testing of Tracked Universal Chassis Passability in Hilly Mountainous Orchards. *Agriculture*, Vol. 13, pp. 1458, Switzerland.

[13] Tao, Z. (2024). The design and research of collaborative robots based on Solidworks. *2024 IEEE 3rd International Conference on Electrical Engineering, Big Data and Algorithms (EEBDA)*, pp. 1174-1179, United States.

[14] Upadhyay, A., Zhang, Y., Koparan, C., Rai, N., Howatt, K., Bajwa, S., & Sun, X. (2024). Advances in ground robotic technologies for site-specific weed management in precision agriculture: A review. *Computers and Electronics in Agriculture*, Vol. 225, pp. 109363, Netherlands.

[15] Yang, T., Jin, C., Ni, Y., Liu, Z., & Chen, M. (2023). Path Planning and Control System Design of an Unmanned Weeding Robot. *Agriculture*, Vol. 13, Article 2001, Switzerland.

[16] Yang, Z. (2023). Design and experimental study of an agricultural seeding robot (农业播种机器人的设计及试验研究). *Southern Agricultural Machinery*, 54(5), 59–61.

[17] Yao, L., Yuan, H., Zhu, Y., & et al. (2023). Design and testing of a wheeled crop-growth-monitoring robot chassis. *Agronomy*, Vol. 13, pp. 3043, Switzerland.

[18] Zhang, L.A., Tang, K., Zhao, Y.J., Wang,X.Y., Yu,D.Z. (2020). Optimization of leg structure parameters for a quadruped laser weeding robot (四足激光除草机器人腿部结构参数优化). *Transactions of the Chinese Society of Agricultural Engineering*, 36(2), 7–15.

[19] Zhang, Z., He, W., Wu, F., Quesada, L., & Xiang, L. (2024). Development of a bionic hexapod robot with adaptive gait and clearance for enhanced agricultural field scouting. *Frontiers in Robotics and AI*, Vol. 11, pp.1426269, Switzerland.

[20] Zhao, X., Yang, J., Zhong, Y., & et al. (2024). Study on chassis leveling control of a three-wheeled agricultural robot. *Agronomy*, Vol. 14, pp. 1765, Switzerland.

[21] Zhou, L., Hu, C., Chen, Y., Guo, P., Liu, J., Chen, Y., & Cao, J. (2024). Research on a chassis stability control method for high-ground-clearance self-propelled electric sprayers. *Applied Sciences*, Vol. 14, pp. 7734, Switzerland.